A dynamical adjustment perspective on extreme event attribution

Laurent Terray[1]

[1]CECI, Université de Toulouse, CERFACS/CNRS, Toulouse, France

Correspondence to: Laurent Terray (terray@cerfacs.fr)

5 **Abstract.**

Here we demonstrate that dynamical adjustment allows a straightforward approach to extreme event attribution within a conditional framework. We illustrate the potential of the approach with two iconic extreme events that occurred in 2010: the early winter European cold spell and the Russian summer heat wave. We use a dynamical adjustment approach based on

10 constructed atmospheric circulation analogues to isolate the various contributions to these two extreme events using only observational and reanalysis datasets. Dynamical adjustment results confirm previous findings regarding the role of atmospheric circulation in the two extreme events and provide a quantitative estimate of the various dynamic and thermodynamic contributions to the event amplitude. Furthermore, the approach is also used to identify the drivers of the recent 1979–2018 trends in summer extreme maximum and minimum temperature changes over western Europe and western

15 Asia. The results suggest a significant role of the dynamic component in explaining temperature extreme changes in different regions, including regions around the Black and Caspian Seas as well as central Europe and the coasts of western Europe. Finally, dynamical adjustment offers a simple and complementary storyline approach to extreme event attribution with the advantage that no climate model simulations are needed, making it a promising candidate for the fast-track component of any real-time extreme event attribution system.

20 **1 Introduction**

Extreme weather events such as heat waves and cold spells have a profound impact on human health (Guo et al. 2018; Robine et al. 2008), natural ecosystems (Stillman 2019), social systems and economy (Jahn 2015). Europe has experienced a high number of extreme temperature episodes since the early 2000s. Recent examples include the summer 2003 heat wave over western Europe, the summer 2010 heat wave over eastern Europe and Russia, the 2010 cold winter over Europe, the

25 2012 cold spell over eastern and northern Europe, the summer 2015 heat wave over southern and central Europe and the summer 2018 heat waves over North-western and Central Europe. Science questions related to the origin, causal and amplifying factors as well as predictability and prediction of these events have led to an unprecedented number of studies in the last 20 years, with 2003 being perhaps the starting point of this intense wave of research activity (Stott et al., 2004). This

emerging field of research is often referred as extreme event attribution, although it often covers a range of questions and
30   issues that go beyond the standard attribution framework (Hegerl et al., 2011; Lloyd and Shepherd, 2020).

Recent and exhaustive review papers have nicely summarized the multiple modelling and statistical approaches and framings
that have been used in the field of extreme event attribution (Stott et al., 2016; Shepherd 2016; Otto 2017; Naveau et al.,
2020). A first type of approach, (from now on the risk-based approach) is focusing on estimating and comparing the
35   frequency of occurrence of extreme events under two stationary worlds, the factual one (with the effect of human influence
on climate) and the counterfactual one (with no human influence on climate). A second type of approach (thereafter the
process-based or storyline approach) puts more emphasis on the identification of the physical drivers of extreme events.
Within this second approach, the main objective is to quantify the influence of the key causal factors of the extreme event
under scrutiny rather than estimating changes in the likelihood of the event due to human influence (see Wehrli et al., 2019
40   for a perfect example of the process-based approach). Both risk- and process-based approaches can often be combined in
some ways to improve the understanding and robustness of extreme event attribution results (Otto et al., 2012).

Within the process-based approach, the quantification of the driver's influence often relies upon model sensitivity
experiments to disentangle the impact of each causal factor. Different modelling frameworks can be used (Schär and Kröner,
45   2017; Wehrli et al., 2019): the first one is based on "all-but-one" experiments where the influence of one specific factor is
removed from the control simulation setup (here control simulation means a simulation including the influence of all
factors). The second one, based on "only-one" experiments, goes in the other direction by accounting for the influence of a
specific causal factor in a control simulation (with all other factor's influence removed).

50   A subset of the process-based approach uses the fact that the vast majority of extreme events (in particular at mid-to-high
latitudes) are associated with specific (but not necessarily extreme) atmospheric circulation patterns. Conditioning the
observed temperature or precipitation extreme variations on the appropriate circulation pattern naturally leads to decompose
the extreme event characteristics (such as amplitude and persistence) into dynamic and thermodynamic components. As the
two components have very different signal-to-noise ratios related to the response to anthropogenic forcing, extreme event
55   attribution results can be notably strengthened by focusing separately on the two aspects (Shepherd, 2016; Vautard et al.,
2016).
The above decomposition can easily be performed based on atmospheric circulation nudging experiments for different mean
climate states corresponding to contrasted values of the thermodynamic drivers (either external forcings or internal
variability factors). For instance, Wehrli et al. (2019) quantify the influence of sea surface temperatures (SSTs) and soil
60   moisture to five recent heatwaves in both tropical and extratropical regions using global atmospheric simulations with
atmospheric circulation nudged to reanalysis (using grid-point nudging). Based on nudged regional model experiments,
Meredith et al. (2015) have shown that Black Sea SST recent warming has been a key contributor and amplifier in the

magnitude of the Krymsk July 2012 precipitation extreme. Another recent example about heat wave attribution is the

application of a methodology based on spectral nudging of the free atmosphere within a global model and applied to both

65   factual and counterfactual worlds (van Garderen et al., 2021).

An alternative approach to model-based studies is to apply a dynamical adjustment diagnostic approach to observations

and/or reanalyses. Dynamical adjustment methods have initially been developed to illustrate and quantify the role of

70   atmospheric internal variability on long-term temperature regional trends (Wallace et al., 2012; Smoliak et al., 2015; Guan et

al., 2015; Deser et al., 2016; Saffioti et al., 2016; Gong et al., 2019; Sippel et al., 2019). They have also been applied in

other contexts such as attribution studies of regional precipitation changes (Guo et al., 2019; Lehner et al., 2018), time of

emergence uncertainties (Lehner et al., 2017), influence of low-frequency oceanic modes on continental climate (O'Reilly et

al., 2017) and land-atmosphere interaction studies (Merrifield et al., 2017). The dynamical adjustment method pioneered in

75   Deser et al. (2016) is based on the constructed analogue approach and was initially applied using monthly mean sea level

pressure and temperature fields.

Here we investigate the possible added value of the constructed analogue dynamical adjustment approach in identifying and

disentangling the key drivers and related physical processes of extreme events. We first use dynamical adjustment to assess

80   the contribution of atmospheric circulation and other drivers to two specific and iconic extreme events: the 2009–2010 cold

European winter (Wang et al., 2010; Cattiaux et al., 2011; Osborne 2011) and the 2010 Russian heat wave (Barriopedro et

al., 2011; Dole et al., 2011). The analysis is performed at daily time scales for the two events allowing to yield insights on

both the chronology and time-mean aspects. One key advantage of the dynamical adjustment approach is that it can be used

with observational (and/or reanalyses) data without the need of additional atmospheric (or climate) model simulations.

85   Observational uncertainty estimates can be derived by using multiple products and/or perturbed-parameter observational

ensemble. Uncertainty related to the dynamical adjustment method parameters can be estimated by adequate sampling of the

latter. Finally, the approach can be used for any type of event as long as high-quality observational daily datasets of both

atmospheric circulation and the physical variable of interest are available for a sufficiently long common period (at least 30

years).

90

The second objective of this study is to revisit the attribution of the links between recent changes in atmospheric circulation

patterns and the increased occurrence of summer hot temperature extremes over several midlatitude regions (Horton et al.,

2015; Jézéquel et al., 2018, 2020). We first apply dynamical adjustment at daily time scale to all summer days of the 1979–

2018 period for both maximum (TX) and minimum temperature (TN). We then identify maximum and minimum temperature

95   extreme hot days for every summer of the 1979–2018 period and estimate changes in temperature extremes as well as the

role of atmospheric circulation in these changes based on the dynamical adjustment results. We focus on two specific

regions, loosely defined as western Europe (from 35° N to 65° N and 15° W to 25° E) and western Asia (from 35° N to 65°
N and 25° E to 60° E). Horton et al. (2015) have attributed a fraction of the increase in the occurrence of summer hot
extreme days for these two regions to an enhanced occurrence frequency and–or persistence (and/or duration) of anticyclonic
100   circulation patterns during the 1979–2013 period. Here we assess whether a different but complementary approach can be
used to investigate whether atmospheric circulation changes have contributed to changes in maximum and minimum
temperature summer extremes over a slightly extended period (1979–2018). We restrict our analysis to hot (*TX* maxima) and
cold (*TN* minima) summer extremes.

105   The paper is organized as follows. Section 2 describes the observational and reanalyses datasets and the methodological
aspects of the dynamical adjustment approach. Section 3 presents the results for the two illustrative extreme events and a
comparison with other approaches based on published results. Based on the dynamical adjustment approach, section 4 then
investigates the possible contribution of changes in atmospheric circulation patterns to the recent (1979–2018) increase in
summer hot and cold extremes over western Europe and western Asia. Finally, section 5 gives a short summary and possible
110   directions for future work.

2 Material and Methods

2.1 Observational and reanalyses datasets

2.1.1 Mean sea level pressure data from reanalyses

We mainly use daily mean sea level pressure (*SLP*) from the from the 2° × 2° Twentieth Century Reanalysis version 3
115   (20CRV3, Slivinski et al., 2019) from 1836 to 2015 to characterize atmospheric circulation patterns and their link with
temperature extremes. The data are extended through 2018 with ERA-Interim (ERAI ; Dee et al. 2011) by adding daily
ERAI anomalies to the daily 20CRV3 climatology (based on the 1979–2015 period which is the common period between
ERAI and 20CRV3). We also use daily *SLP* data from 20CR version2c (Compo et al., 2011), also extended through 2018
with ERAI. For both 20CRV3 and 20CR_V2C, we only use daily *SLP* data from 1900 to 2018 due to the sparsity of the
120   observational record in the 19th century. Finally, we also make use of the NCAR/NCEP-R1 (Kalnay et al., 1996) on the
shorter period (1948–2018) to further assess the sensitivity of the dynamical adjustment results to the choice of atmospheric
reanalysis for the sea level pressure field.

2.1.2 Temperature datasets

The Berkeley Earth temperature (BERK) daily datasets are experimental products
125   ([http://berkeleyearth.lbl.gov/auto/Global/Gridded/Gridded_Daily_README.*Tx*t](http://berkeleyearth.lbl.gov/auto/Global/Gridded/Gridded_Daily_README.Txt)) and are available from 1880-01-01 to
2018-12-31. The BERK datasets are homogenized daily temperature fields built as a refinement upon their monthly

temperature datasets (Muller et al. 2013; Rohde et al. 2013) and using similar techniques. The gridded data are provided on a regular latitude-longitude grid at 1-degree resolution. We only consider temperature data over the 1900–2018 period to match the period chosen for mean sea level pressure.

130   The EOBS daily land surface air temperature gridded datasets are also used over western Europe. The homogeneous EOBS dataset (version19.0eHOM) is available from 1950-01-01 to 2018-11-30 (Cornes et al. 2018; Squintu et al. 2019). The raw station data are first homogenized using a quantile matching technique (Squintu et al. 2019). The gridded temperature data is provided on a regular latitude-longitude grid at 0.25-degree resolution (https://www.ecad.eu/download/ensembles/downloadversion19.0eHOM.php#datafiles). The data is provided for a

135   geographical domain from 25° N to 71.5° N and from 25° W to 45° E.

The HadGHCND global product has been created based on daily station observations from the Global Historical Climatology Network-Daily database (Caesar et al., 2006). This consists of over 27,000 stations with temperature observations, though the temporal and spatial coverage of the record is very variable. Quality control has been carried out to indicate potentially spurious values. The temperature data is provided as anomalies relative to the 1961–1990 reference

140   period. The HadGHCND dataset spans the years 1950 to 2014 and is available on a 2.5° latitude by 3.75° longitude grid.

The BERK and EOBS datasets are used as our reference temperature datasets. HadGHCND as well as the NCEP reanalyses are also used to complement the observational uncertainty analysis for temperature. Unless explicitly mentioned, all *TX* and *TN* anomalies are calculated relative to the 1981–2010 reference period.

145   **2.2 Dynamical adjustment based on constructed analogues**

The dynamical adjustment used in this study is a straightforward adaptation to daily time scales of the method introduced in Deser et al. (2016). The main objective of dynamical adjustment is to derive an estimate of the component of any physical variable variability due solely to atmospheric circulation changes. In agreement with many previous studies, we assume that robust forced circulation changes over the North Atlantic European domain are not currently detectable due to a small signal-

150   to-noise ratio. Consequently, observed circulation changes are considered as being an integral part of climate internal variability. In the following and for the sake of concision, we refer to any variable changes due to atmospheric circulation as to the dynamic component (instead of the internal dynamic component). Here, *SLP* is used to represent atmospheric circulation changes and we use *TX* as our physical variable in the method description. Consequently, dynamical adjustment leads to the decomposition of any daily *TX* anomaly between a *TX* dynamic component and a residual (loosely described as

155   the "thermodynamic residual" or simply the thermodynamic component). Note that the thermodynamic component may include both forced and internal contributions.

We now briefly summarize the dynamical adjustment algorithm. We first define two different geographical domains for *TX* and *SLP* with the constraint that the *TX* domain has to be enclosed within the *SLP* one. For any day d_i of the extreme event,

160 we search for the closest N_a daily *SLP* analogues in all years (but the one of the extreme event occurrence) within a time window of ± *N* days centered on d_i (*N* being typically ~ 15 days). The *SLP* analogues are ranked according to the Teweless-Wobus skill score. The score measures the similarity between the *SLP* horizontal gradients (i.e geostrophic winds). We then randomly subsample (without replacement) N_s of the N_a *SLP* analogues and compute their best linear fit (see Appendix of Deser et al., 2016 for details) to the target *SLP* field (that of day d_i). The dynamically-reconstructed *TX* is then defined as the

165 corresponding linear combination of daily *TX* anomalies associated with the N_s *SLP* analogues. Next, we repeat this random subsampling procedure N_r times. Finally, we average the N_r optimal sets of reconstructed daily *SLP* analogues and associated *TX* to obtain the dynamic component, defined as the ''best estimate'' of the circulation-induced component of maximum temperature anomaly for the day d_i. This sequence of steps is finally repeated for all days of the extreme event under consideration. Uncertainty estimates can be derived with a simple bootstrap procedure applied to the set of N_r estimates of

170 the *TX* dynamic component. We randomly draw (with replacement) N_r estimates 1000 times to produce a distribution that can then be used to derive a 95 % confidence interval.

All results shown below are based on the following parameter values: N_a = 400, N_s = 200 and N_r = 100 (see parameter sensitivity tests in Appendix A). As we are interested in separating the *TX* dynamic component from any forced

175 thermodynamic residual (due for instance to changes in the external forcing), we need to remove a local estimate of the forced *TX* component before applying dynamical adjustment. In a sense, the *TX* dynamic component (DYN_{CF} thereafter) represents the effect of atmospheric circulation on the *TX* anomaly in the counterfactual world (the world with no human influence on climate). As one of the objectives of this approach is to rely exclusively on observations (and/or reanalyses), we apply a Loess-based smoother (see section 2.3) to *TX* daily observations to remove the low-frequency trend (for all grid-

180 points) that we hypothesize to be primarily due to external forcing (Hawkins et al. 2020; Section 2.3).

Our physical interpretation of the *TX* dynamic component is that it represents the "mean" contribution of the atmospheric circulation pattern, including both direct (advection) and indirect (e.g local feedbacks) effects, in the counterfactual world. Here, the use of "mean" is simply associated with an average over multiple linear combinations of *TX* anomalies arising

185 from a large of number of days having different ocean and/or land surface conditions.

We then interpret the residual component (RES_{TOT}) as being the sum of three contributions. The first one (RES_{FRC}) is the externally-forced *TX* component that has been removed before applying dynamical adjustment. The residual component also includes any *TX* changes due to a local or remote contribution associated with internal variability (RES_{INT}). For example, the

190 local contribution includes local processes such as those associated with land surface feedbacks linked to soil moisture or snow cover anomalies. The remote contribution includes any *TX* change related to thermal advection changes due to mean flow advection of anomalous zonal and meridional *TX* gradients caused by internal variability (for example due to anomalous oceanic air masses). The last contribution (RES_{ADV}) is related to thermal advection changes related to externally-

forced changes in zonal and meridional TX gradients. The estimation of RES_{INT} and RES_{ADV} can be obtained by running the
dynamical adjustment twice: firstly, with the TX forced response removed (as previously described) and secondly with the
observed raw TX. The RES_{ADV} contribution can then be estimated by subtracting the former TX dynamic component (from
the counterfactual world) from the latter one (from the factual world). Finally, RES_{INT} can be estimated as:

$$RES_{INT} = RES_{TOT} - RES_{FRC} - RES_{ADV} \qquad (1)$$

The final decomposition of any daily TX anomaly (TX_A) can then be written as:

$$TX_A = DYN_{CF} + RES_{INT} + RES_{FRC} + RES_{ADV} \qquad (2)$$

With the objective to compare with model-based studies (see section 3.2), it is also useful to define a "total" dynamic
contribution DYN_{TOT} given by:

$$DYN_{TOT} = DYN_{CF} + RES_{ADV} \qquad (3)$$

2.3 Estimation of the forced response

We assume that the temperature forced response to external forcing can be simply estimated with a low-frequency trend
estimated over the 1900–2018 period. The latter is estimated with a Loess smoother (Cleveland et al., 1990) as implemented
in the NCSTAT package (https://terray.locean-ipsl.upmc.fr/ncstat/index.html). We choose a smoother length of 45 years and
we apply a light (~ 2 years) additional smoothing of the trend before estimating the residual. Iterations are carried out until
convergence of the trend, which is reached when maximum changes in individual trend fits are less than 1 % of the trend's
range after the previous iteration. We detrend the daily TX and TN datasets separately for each month before applying the
dynamical adjustment procedure and estimating the dynamic component.

3 Results for individual extreme events

As our illustrative examples, we choose two seasonally contrasted extreme events that have been widely documented in the
literature: the cold European winter of 2009–2010 and the 2010 Russian summer heatwave. For the Russian heatwave, we
follow previous studies by focusing on the July 15th – August 14th period. For the cold European winter, we choose a two-
week period between December 28th 2009 and January 13th 2010 that is associated with record-breaking temperatures in
many midlatitude land masses of the Northern Hemisphere (Wang et al., 2010). We restrict our analysis to the TX variable.
For each illustrative example, we first describe the synoptic circulation and associated TX anomalies during the event before
showing the dynamical adjustment results averaged over all event days. We then briefly discuss the chronology of the event

225 and the evolution of the *TX* dynamic component. We use 20CRV3, BERK and EOBS as primary datasets for our dynamical adjustment analysis and figures in the main text. Specifically, we use EOBS for the 2010 winter event and BERK for the summer one (note that the EOBS geographical domain does not cover Russia). Results based on the other *TX* and *SLP* datasets are shown in Tables 1 and 2.

3.1 The 2009-2010 European winter cold spell

230 Winter 2010 is characterized by an extreme negative phase of the North Atlantic Oscillation (NAO) (the classical NAO index reaches a value of 3 standard deviation below average, see Cattiaux et al., 2010 and Osborn 2011). In the eastern Atlantic the winter (December–February) mean eddy-driven jet was displaced southward by almost 10 degrees compared with its climatological position and maintained south by diabatic heating feedbacks (Woollings et al., 2016). Averaged *SLP* anomalies during the extreme event period (December 28th 2009 – January 13th 2010) display a dipole with large positive
235 anomalies over the north-western Atlantic and negative ones over the central eastern Atlantic, in agreement with a jet stream axis located over Northern Africa (Fig.1a). Importantly, the reconstructed *SLP* pattern is almost identical to the original observed *SLP* pattern (Fig.1c). This anomalous *SLP* pattern strongly projects onto the negative NAO pattern. Negative NAO phases are known to lead to cold temperature over western and northern Europe (Hurrell 1995). The spatial pattern of the *TX* anomaly during the cold spell displays an elongated cold *TX* anomaly over the United Kingdom and northern Europe
240 contrasting with warm *TX* anomalies in Northern Africa and the Middle East (Fig.1a). The magnitude of the mean *TX* anomaly for the cold spell event – regionally averaged over the European domain (see box in Fig. 1c) – is -2.04 °C based on EOBS. As expected, the dynamic component contribution to the *TX* anomaly is negative and has a larger magnitude than the total (-2.76 °C). In particular, the dynamic component displays very cold (~ -5 °C) *TX* anomalies over northeastern Europe (Fig. 1b). The total residual contribution is positive (Fig. 1c) and has a smaller amplitude (0.72 °C) than the dynamic
245 component due to the opposite sign of the internal residual contribution (-0.31 °C, Fig. 1d) and the two forced contributions, the long-term trend (*RES_FRC*: 0.44 °C, Fig. 1e) and the thermal advection component (*RES_ADV*: 0.59 °C, Fig. 1f). The total *TX* forced contribution (defined as the sum of *RES_FRC* and *RES_ADV*) has a significant positive contribution (1.03 °C) and shows increased warming in northern Europe (Fig. 1e-f).

It is noteworthy that the internal residual contribution exhibits cold *TX* anomalies along the coasts of western Europe,
250 perhaps linked to cold and persistent – present in both December 2009 and January 2010 – North Atlantic SST anomalies (Buchan et al., 2014). These SST anomalies may have been the surface signature of a reduced northward ocean heat transport related to a strong decrease of the Atlantic meridional overturning circulation in 2009 (McCarthy et al., 2012; Sonnewald et al., 2013). We speculate that amplitude of these ocean-induced cold SST anomalies has been further enhanced in late winter due to the ocean integration of the recurrent and persistent negative NAO atmospheric forcing.

255
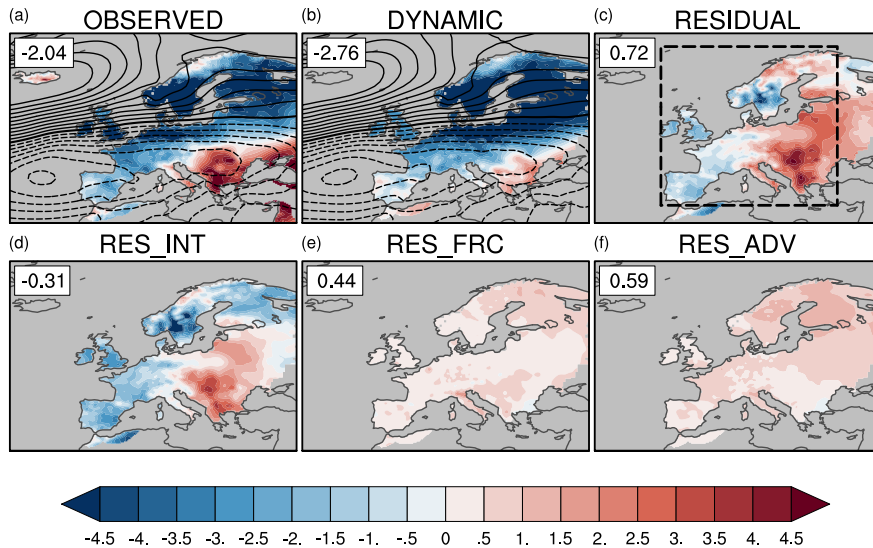
Figure 1: EOBS daily maximum temperature (° C, shading) and 20CR_V3 sea level pressure (hPa, black line contours with contour interval of 1 hPa) anomalies averaged over the European cold spell period (December 28th 2009 – January 13th 2010): **(a)** total *TX* anomaly and observed *SLP* anomaly, **(b)** *TX* dynamic component contribution and reconstructed *SLP* anomaly, **(c)** *TX* total residual contribution, **(d)** *TX* internal residual contribution **(e)** *TX* forced residual contribution, **(f)** *TX* thermal advection residual contribution. Numbers in the upper right corner indicate the weighted average *TX* anomaly over the region delimited by the black dashed box in **(c)**. In **(a)** and **(b)**, the black thick contour line indicates the zero *SLP* anomaly and dashed contour lines indicate negative *SLP* anomalies.

Further inland, the internal residual contribution shows warm *TX* anomalies with maximum values in south-eastern and

265 central Europe (Fig. 1d). We speculate that the Black Sea and Levantine sub-basin warm SST anomalies observed in 2009 and 2010 (in line with the eastern Mediterranean SST warming trend over 1982–2012, Shaltout and Omstedt, 2014) may have contributed to the internal residual warm *TX* anomalies in south-eastern Europe.

These results confirm that the long-term warming (mostly attributed to human influence) has mitigated the extreme character of the 2009-2020 early winter cold spell as initially suggested by Cattiaux et al. (2010). In the counterfactual world, the

270 winter cold spell would have been 1.03 °C (Fig. 1e-f) colder than the observed one (-3.06 °C instead of -2.03 °C). Keeping 20CR_V3C for *SLP*, additional results based on BERK and HadGHCND for *TX* lead to quasi-similar amplitudes for the total anomaly and dynamic component (Table 1). The use of NCEP data for *TX* underestimates the amplitude of the two-week cold spell by 35 %. Using different datasets for *SLP* (20CR_V2C and NCEP) while keeping EOBS for *TX* leads to slightly larger values of the dynamic component.

275

We now illustrate how the dynamical adjustment approach can be used to track the daily evolution of the contribution due to atmospheric circulation changes. The chronology of the early 2010 winter cold spell shows two cold minima, the first one in mid-December and the second one, more intense, two weeks later (Fig. 2a). The dynamic component is by far the main contributor to the *TX* anomaly magnitude daily and weekly variability (as suggested by the similarity of the two timeseries in

280   Fig. 2a). In particular, the two cold minima observed during December 2009 and January 2010 are associated with an
eastward extension of the anticyclonic *SLP* anomalies centered around Iceland that favors the advection of Arctic air masses
towards northern Europe (Fig. 2b). While observed daily NAO index values
(https://www.cpc.ncep.noaa.gov/products/precip/CWlink/pna/nao.shtml) are all negative during the period shown in Fig. 2a
(albeit with different amplitudes) illustrating the persistence of the low-frequency large-scale atmospheric flow, the

285   contribution of the dynamic component to *TX* anomaly exhibit significant daily variability due to the high-frequency part of
the flow. For instance, the circulation-induced and region-averaged *TX* anomaly on December 31st is positive, which
contrasts with the cold minimum observed a few days later and associated with a marked negative NAO phase (Fig. 2).
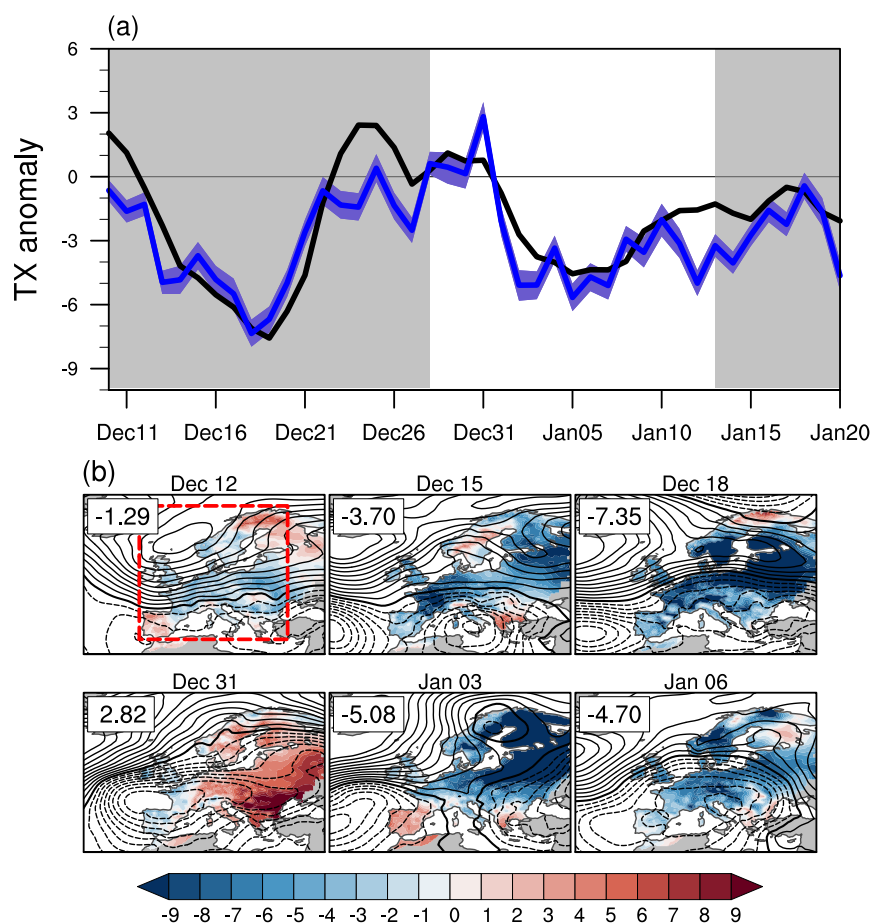
Figure 2: (a) time evolution of EOBS daily maximum temperature (° C) anomaly averaged over the European domain (box with red
290   dashed line in **(b)**). The covered period is from December 10, 2009, until January 20, 2010. The thick black line represents the total *TX*
anomaly. The thick blue line shows the contribution of the dynamic component and the blue shading indicates the 95 % confidence
interval of the reconstruction based on bootstrapping (see section 2.2). The chosen period for the two-week cold spell is defined by the
white background. **(b)** Daily maps of *SLP* anomaly (hPa, black line contours with contour interval of 1 hPa) and of the dynamic
component contribution (°C, shading) to the total *TX* anomaly. The black thick contour line indicates the zero *SLP* anomaly and dashed
295   contour lines indicate negative *SLP* anomalies. Numbers in the upper left corner indicate the region-averaged contribution of the dynamic
component to the total *TX* anomaly.

Table 1: Total *TX* anomaly (°C, in bold) and dynamic component contribution (°C and as a fraction of the total anomaly in percent) averaged over Europe (36° N–72° N; 10° W–30° E) during the 2009–2010 winter cold spell. The reference period is 1981–2010.

SLP *TX*	20CR_V3	20CR_V2C	NCEP
NCEP	**-1.32** – -1.96 (148 %)	**-1.32** – -2.78 (210 %)	**-1.32** – -2.40 (182 %)
HadGHCND	**-2.20** – -2.83 (129 %)	**-2.20** – -3.52 (160 %)	**-2.20** – -3.04 (138 %)
EOBS	**-2.04** – -2.76 (135 %)	**-2.04** – -3.59 (176 %)	**-2.04** – -3.36 (165 %)
BERK	**-1.95** – -2.63 (135 %)	**-1.95** – -3.01 (154 %)	**-1.95** – -3.04 (156 %)

300

3.2 The 2010 Russian summer heatwave

Summer 2010 is characterized by persistent quasi-stationary anticyclonic circulation anomalies over western Russia (Dole et al., 2019; Barriopedro et al., 2010). The persistence of the long-lasting blocking high has been mainly linked to a transition between ENSO warm and cold phases and the resulting changes in quasi-stationary wave anomaly and transient eddies

305 (Schneidereit et al., 2012). These blocking circulation patterns are often associated with surface temperature warm anomalies due to enhanced subsidence, reduced cloudiness allowing a greater fraction of solar radiation to reach the surface and advection of warmer air masses from regions located to the south of the blocks. A late-winter to spring precipitation deficit over western Russia has also likely contributed to the abnormally warm summer maximum temperature anomalies (with a magnitude on the order of ~ 9–10 °C when regionally-averaged over the heat wave period, see Wehrli et al., 2019 and Fig. 3

310 and Table 2) through the concurrent summer drought and associated land-surface feedbacks related to depleted soil moisture content (Miralles et al., 2014). Based on atmospheric model nudging experiments, Wehrli et al. (2019) have estimated dynamic (related to atmospheric circulation changes) changes and other contributions to the Russian heatwave. They suggest that the largest contribution to the Russian heatwave *TX* anomaly can be attributed to atmospheric circulation (range 54–63 %) with a substantial albeit smaller contribution (27–36 %) from antecedent soil moisture conditions (the remaining 10 %

315 being due to the contribution of the response to external forcing, named greenhouse gas forcing in their paper).

Figure 3 shows our estimates of the different contributions based on the dynamical adjustment approach and the BERK dataset. The event total *TX* anomaly for the western Russia region (see box in Fig. 3b) is 9.06 °C and is located southwest of the blocking high maximum (with a *SLP* magnitude of 9 hPa, Fig. 3a). As suggested by previous studies (Dole et al., 2011;

320 Wehrli et al., 2019), we find that the total *TX* anomaly is dominated by the total internal contribution (DYN_{CF} [3.99 °C] + RES_{INT} [3.59 °C]) with the total forced contribution (RES_{FRC} [1.03 °C] + RES_{ADV} [0.45 °C]) being only 16 % of the total *TX*

anomaly (Fig. 3). The magnitude of the total dynamic contribution is 4.44 °C ($DYN_{TOT} = DYN_{CF}$ [3.99 °C] + RES_{ADV} [0.45 °C]; ~ 49 % of the event total anomaly). The other and smaller contributions are the TX forced residual contribution RES_{FRC} (1.03 °C, ~ 11 % of the total) and the internal residual RES_{INT} (3.59 °C, ~ 40 % of the total). Using HADGHCND or NCEP

325 data for TX leads to very similar results in term of the percentage of the dynamic contribution (Table 2). The latter is slightly lower when SLP from the 20CR_V2C and NCEP datasets is used for dynamical adjustment while keeping BERK for TX.
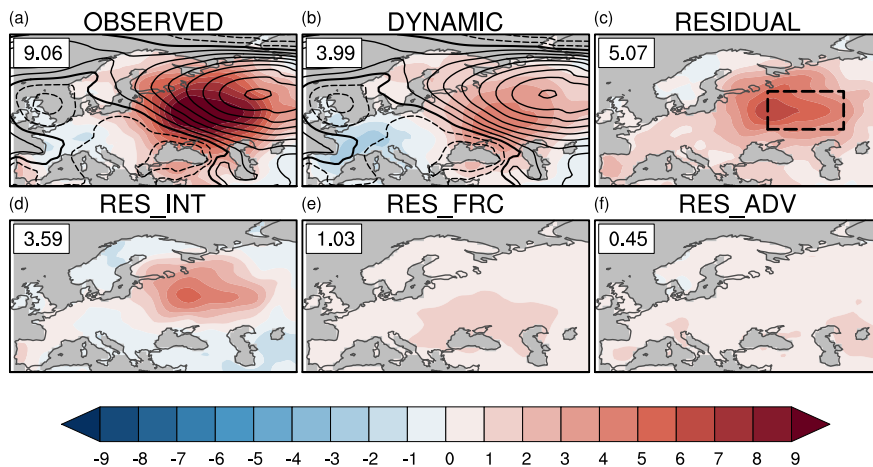
Figure 3: BERK daily maximum temperature (TX, ° C, shading) and 20CR_V3 sea level pressure (SLP, hPa, black line contours with contour interval of 1 hPa) anomalies averaged over the Russian heatwave period (July 15th – August 14th, 2010): **(a)** total TX anomaly and
330 observed SLP anomaly, **(b)** TX dynamic component contribution and reconstructed SLP anomaly, **(c)** TX total residual contribution, **(d)** TX internal residual contribution **(e)** TX forced residual contribution, **(f)** TX thermal advection residual contribution. Numbers in the upper right corner indicate the weighted average TX anomaly over the region delimited by the black dashed box in **(c)**. In **(a)** and **(b)**, the black thick contour line indicates the zero SLP anomaly and dashed contour lines indicate negative SLP anomalies.

Therefore, we find that the total dynamic component yields the dominant contribution to the Russian heatwave TX anomaly,
335 in agreement with the model study of Wehrli et al. (2019). We also note that our best estimate for the total dynamic component contribution (49 % of the total TX anomaly is slightly lower than their minimum estimate (see discussion below). As suggested by many previous studies, it is very likely that anomalous soil moisture is an important contributor to the substantial magnitude of the internal residual contribution (note however that the dynamical adjustment approach cannot be used directly to infer the soil moisture influence, see also the discussion below). The magnitude of the TX forced residual
340 contribution is in reasonable agreement with the model-based estimate (1.2 °C) of Wehrli et al. (2019).

Differences with results from the latter study regarding the magnitude of the dynamic contribution (and consequently, of the thermodynamic residual magnitude) can be due to multiple factors. First, using the same baseline (1982–2008) as Wehrli et al. (2019) doesn't significantly change the contribution of the dynamic component (46 % instead of 49 %). Second, while our methodology only relies on observations and reanalysis, their approach relies upon both "all-but-one" and "only-one"
345 modelling frameworks based on simulated differences between SST-forced historical atmospheric experiments with and without circulation and/or soil moisture nudging and a control simulation without any nudging. Possible caveats of this modelling approach include the lack of validity of the assumption that the different factors are additive, the lack of

interaction between the ocean and the atmosphere and the fact that different soil moisture climatology between simulations
with and without soil moisture nudging can lead to a different response to the same soil moisture anomaly (for a detailed
350   discussion, see Wehrli et al., 2019). Possible sources of uncertainty of the dynamical adjustment results include
observational uncertainty and the presence of "noise" in the internal thermodynamic residual resulting from dynamic
contributions not accounted for by the constructed analogue technique (due to both inadequate sampling as well as
methodological uncertainty). Table 2 shows that the magnitude of the dynamic component for different observational and
reanalysis products is always less than 50 % of the total *TX* anomaly. This suggests that differences in magnitude of the
355   dynamic component discussed above are unlikely to be fully explained by observational uncertainty in the dynamical
adjustment method.
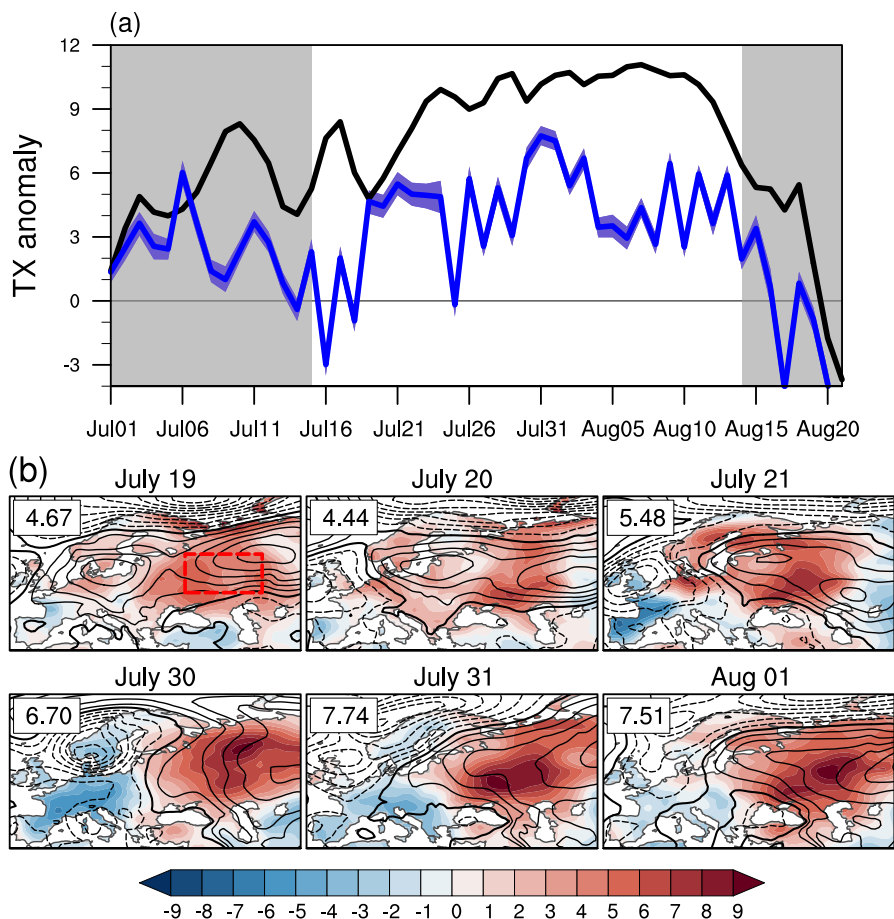
Figure 4: (a) time evolution of BERK daily maximum temperature (° C) anomaly averaged over the Western Asia domain (box with red
dashed line in **(b)**). The covered period is from July 1st, 2010, until August 20th, 2010. The thick black line represents the total *TX* anomaly.
360   The thick blue line shows the contribution of the dynamic component and the blue shading indicates the 95 % confidence interval of the
reconstruction based on bootstrapping (see section 2.2). The chosen period for the Russian heatwave is defined by the white background.
(b) Daily maps of *SLP* anomaly (hPa, black line contours with contour interval of 1 hPa) and of the dynamic component contribution (°C,
shading) to the total *TX* anomaly. The black thick contour line indicates the zero *SLP* anomaly and dashed contour lines indicate negative

365 *SLP* anomalies. Numbers in the upper left corner indicate the region-averaged contribution of the dynamic component to the total *TX* anomaly.

The chronology of the Russian heatwave suggests that the contribution of the dynamic component to the total *TX* anomaly varies at daily timescale (Fig. 4a). As expected, the dynamic component seems to play a key role in the initiation and termination of the heatwave. In particular, the negative contribution from the dynamic component after August 15th is leading by a couple of days the decline of the extreme heat. During the heatwave, two multi-day periods (July 19–23 and

370 July 30 – August 1) show persistent and high values of the *TX* dynamic component (Fig. 4b). The first one (the less extreme) is associated with a zonally-extended anticyclonic anomaly from the European Coasts to western Russia. The largest contributions of the dynamic component appear to be associated with a strong blocking High center situated eastward of the location of maximum *TX* anomaly.

375 **Table 2:** Total *TX* anomaly (°C, in bold) and dynamic component contribution (°C and as a fraction of the total anomaly in percent) averaged over western Russia (50° N–60° N; 35° E–55° E) during the 2010 summer Russian heat wave. The reference period is 1981–2010.

SLP ⟍ TX	20CR_V3	20CR_V2C	NCEP
NCEP	**10.16** – 3.85 (38 %)	**10.16** – 3.67 (36 %)	**10.16** – 3.05 (30 %)
HadGHCND	**9.16** – 3.75 (41 %)	**9.16** – 3.51 (38 %)	**9.16** – 3.31 (36 %)
BERK	**9.06** – 3.99 (44 %)	**9.06** – 3.07 (34 %)	**9.06** – 3.2 (35 %)

4 Atmospheric circulation contribution to recent changes in summer temperature hot and cold extremes

We now use dynamical adjustment to assess the possible changes in circulation-related temperature anomalies and their

380 contribution to summer temperature hot extreme changes during the 1979–2018 period. We select two Northern Hemisphere midlatitude regions, western Asia (*TX*, *TN* domain: 35° N–65° N; 25° W–60° W; *SLP* domain: 25° N–80° N; 10° W–65° W) and western Europe (*TX*, *TN* domain: 15° E–25° W; 35° N–70° N; *SLP* domain: 30° E–45° W; 25° N–80° N), and apply the dynamical adjustment separately to each of them. The focus is on the contribution of the dynamic component to changes in the summer warmest day (*TX* maxima) and warmest night (*TN* maxima) temperature over these four decades. The initial step

385 is to run the dynamical adjustment procedure for all summers during the 1979–2018 period and for both *TX* and *TN*. As with the two illustrative examples, we apply the dynamical adjustment procedure twice, with and without detrending, before applying dynamical adjustment. For each year and each grid-point, we then select the days with the largest (smallest) *TX* (*TN*) anomalies. In the following, we focus on the summer days and nights with the most extreme temperature: the days with the hottest maximum (*TXx*) and minimum (*TNx*) temperature. We then estimate changes in *TXx* and *TNx* during 1979–2018

390 by using the non-parametric Mann-Kendall test and Theil-Sen's estimator to calculate the trend. Based on dynamical

adjustment results, we also quantify the contribution of both total dynamic (DYN_{TOT}, see Eq. (3)) and thermodynamic residual ($RES_{INT} + RES_{FRC}$) components to these changes.

We find warming trends for both *TXx* and *TNx* over large parts of the western Asia (WA) and western Europe (WE) regions
395 (Figs. 5a, d and 6a, d). The warming of *TXx* over most of the WA region (often greater than 3 °C 40 yr^{-1}) is primarily due to the thermodynamic component with an additional and substantial contribution from the dynamic component north of the Black and Caspian Seas (Fig. 5b, c). Both thermodynamic and dynamic components contribute to the lack of statistical significance and small amplitude of the *TXx* trends found in the northeastern part of the WA region.

Warming trends in *TNx* are statistically significant only in a small region located south of the Black Sea while the eastern
400 part of the WA region exhibits significant cooling with contribution from both components (Fig. 5d–f). In addition, the lack of significant *TNx* trends over most of the WA region results from opposite effects from the thermodynamic (cooling) and dynamic (warming) component. This contrasts with the *TXx* case, supporting the existence of different processes governing the changes in *TXx* and *TNx*.
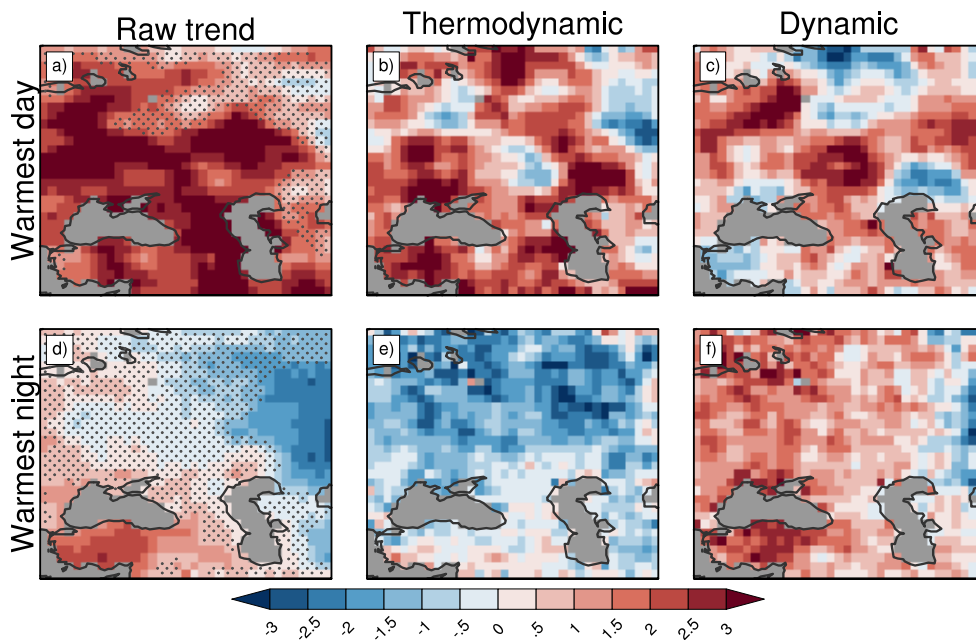
405

Figure 5: Summer temperature extremes: 1979–2018 trend maps for western Asia based on BERK (trend unit is ° C 40 yrs $^{-1}$, shading): (a-c) *TXx* raw trend, *TXx* thermodynamic and dynamic component trends. (d-f) *TNx* raw trend, *TNx* thermodynamic and dynamic component trends. The trend detection is estimated using the non-parametric Mann-Kendall test and the linear trend slope is computed based on the Theil-Sen estimator. In (a, d), stippling indicates locations where the raw trend is not significant at the 5 % level.

410

Regarding the WE region, the *TXx* trend map shows maximum warming (often greater than 3 °C 40 yr⁻¹) located over the central part of the domain and along the coasts of western Europe. This contrasts with most of southern Europe and Scandinavia where *TXx* trends are weaker and not statistically significant (Fig. 6a). Regions with significant *TXx* trends show different relative contributions from dynamic and thermodynamic components (Fig. 6a, c). Interestingly, the contribution of the dynamic component to the total trend is substantial over many locations, including northwestern Spain and France, northeastern Europe (east of the Baltic Sea) and northern Scandinavia (Fig. 6c). The *TNx* trend map shows widespread warming over western Europe and reduced amplitude compared with that of *TXx*, except for Italy and Greece, where the large trend values are mainly due to the thermodynamic component (Fig. 6d–f). Over the central Europe domain, both components contribute to the *TNx* warming with the contribution of the dynamic component being slightly dominant particularly over southern France, eastern Europe and Scandinavia (Fig. 6f).
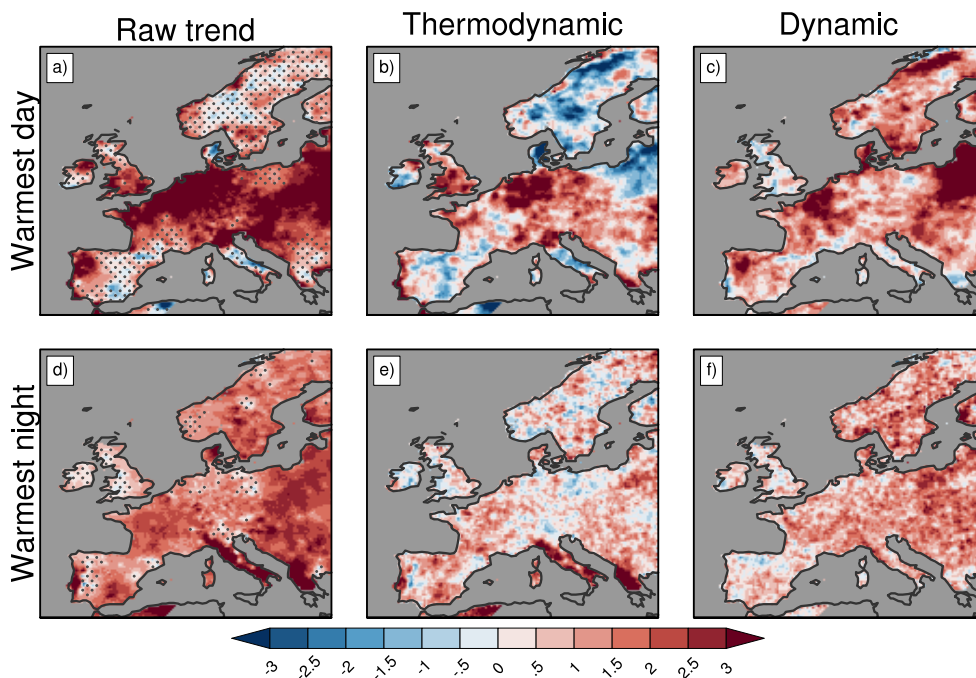
Figure 6: Summer temperature extremes: 1979–2018 trend maps for western Europe based on EOBS (trend unit is ° C 40 yrs ⁻¹, shading): **(a-c)** *TXx* raw trend, *TXx* thermodynamic and dynamic component trends. **(d-f)** *TNx* raw trend, *TNx* thermodynamic and dynamic component trends. The trend detection is estimated using the non-parametric Mann-Kendall test and the linear trend slope is computed based on the Theil-Sen estimator. In **(a, d)**, stippling indicates locations where the trend is not significant at the 5 % level.

We find that the dynamic component has substantially contributed to the increase in the summer *TX* and *TN* hottest extreme over parts of the WA and WE regions. The regions where the dynamic component is an important contributor to the *TX* warming trend broadly correspond to the ones suggested in Horton et al. (2015). This is especially noticeable for western Asia (see their figure 4i) where Horton et al. (2015) attributes a portion of the *TX* hottest extreme trend to an increase in blocking pattern occurrence (note that the trend spatial patterns shown in Figs. 5 and 6 and corresponding to the full period 1979–2018, are qualitatively similar to those for the reduced period 1979–2013 that is used in Horton et al., 2015, not

shown). Increase in the occurrence of anticyclonic patterns mainly located in central Europe was also linked to the observed increase in the *TX* hottest extreme in eastern Europe (Fig. 3c, k of Horton et al. 2015). Our analysis confirms this result and suggests that the dynamic component has also been an important driver of the *TX* hottest extreme warming over many

435   coastal areas of western Europe when considering the extended period up to 2018.

5 Summary and discussion

The dynamical adjustment approach based on the constructed analogue method and extended at daily time scale has been used to assess the contribution of circulation-related temperature anomalies to temperature extreme events. Based on daily maximum temperature, two observed iconic extreme events have been selected to illustrate the potential of the approach: the

440   early 2009–2010 winter European cold spell and the 2010 Russian heat wave. Dynamical adjustment results confirm the key role and improve the quantification of the atmospheric circulation contribution (the dynamic component) to the two extreme events. The 2009–2010 winter European cold spell associated with an extreme negative NAO phase would have been significantly colder without human influence that mitigated the region-averaged amplitude of the cold extreme event by 50 %. Regarding the Russian heatwave, the contribution of the total dynamic component associated with persistent anticyclonic

445   conditions during the 2010 summer is estimated to be close to 50 % of the observed maximum temperature anomaly.
Furthermore, we have used the dynamical adjustment approach to assess the possible contribution of atmospheric circulation to changes in summer extremes for two regions, western Asia and Europe, and during the 1979–2018 period. The dynamical adjustment results suggest that both dynamic and thermodynamic factors have contributed to observed changes in summer temperature extremes over the 1979–2018 period. We have focused on changes in the summer warmest day and night

450   temperatures. Although thermodynamic influence has dominated the *TXx* changes in a large fraction of the western Asia domain, the dynamic influence has been quite substantial north of the Black and Caspian Seas. Furthermore, the dynamic influence has been key in the *TNx* warming trend depicted south of the Black Sea. Regarding Europe, the influence of atmospheric circulation has been a major driver of both *TXx* and *TNx* warming trends that are seen in many regions, including the coasts of western Europe (*TXx*), Scandinavia and eastern Europe (both *TXx* and *TNx*).

455

Dynamical adjustment provides a quick and cheap (computationally) observationally-based storyline approach to assess and quantify the role of atmospheric circulation as a driver of extreme events. Dynamical adjustment can be performed in both factual and counterfactual (the world without human influence) worlds, assuming that the counterfactual can be simply defined by removing a non-parametric trend to the observed climate surface variable under scrutiny (here *TX* and *TN*). Note

460   that, in principle, the contribution of forced atmospheric trends can also be estimated by dynamical adjustment (Deser et al., 2016). Assuming that a forced atmospheric trend can be detected and robustly estimated, dynamical adjustment can be performed twice, by removing or not the *SLP* trend from the raw *SLP* data. Difference between the two results for the reconstructed surface variable gives an estimate of the contribution of the forced dynamic component. In the standard

conditional approach used here, the hypothesis is that forced dynamical changes are undetectable and no detrending is

465   performed on the *SLP* field. In this case, the above dual approach (performing the dynamical adjustment on both factual and counterfactual worlds for the surface variable, here *TX* or *TN*) allows to partition the extreme event temperature anomaly in four contributions: the (internal) dynamic component, the (internal) thermodynamic residual, the forced thermodynamical changes and the contribution due to the mean advection of forced changes in temperature gradients.

470   The above dynamical adjustment decomposition can then be used to present the approach results from two different perspectives: forced versus internal or dynamic versus thermodynamic. Comparison with other model-based methods, for instance those using spectral nudging, can then be performed from one or the other perspective. For example, van Garderen et al. (2021) use the spectral nudging method (with the ECHAM6 atmospheric model and the NCEP reanalysis) to make attribution statements regarding the 2010 Russian heatwave (their table 2). They focus on the role of climate change on the

475   heatwave amplitude in early August (domain-averaged anomaly ~10 °C according to their estimate, relative to a 1985–2015 climatology). Based on their model results, they estimate that the heatwave amplitude can be split in two contributions, ~8 °C due to internal variability and ~2 °C being anthropogenically-forced. Assuming that the early August period can be taken as the first two weeks of August, the dynamical adjustment approach using *SLP* from the NCEP reanalysis gives a region-averaged heatwave anomaly of 9.9 °C with 8 °C and 1.9 °C from the contributions of internal variability and anthropogenic

480   forcing, respectively (here we use the same climatological period as van Garderen et al. (2021)). Interestingly, despite the fact that the two approaches rely on very different methodology and data, their results on the relative influence of internal variability and anthropogenic forcing on the region-averaged heatwave anomaly are remarkably similar.

The dynamical adjustment methodological framework proposed in this study provides a simple and practical approach to

485   investigate and quantify the role of atmospheric circulation in specific extreme events as well as long-term changes in extreme indicators. Combined with model-based approaches, dynamical adjustment results can improve the understanding and interpretation of observed extreme events with minimal effort in term of computing. Application to other climate parameters (for example precipitation extremes) and regions will be pursued in future work.

Appendix A

490   **Method parameter sensitivity tests**

Sensitivity tests have been performed to support the final choice of the dynamical adjustment code parameters. We focus here on two of the parameters: the number of subsampled analogues, N_s, and the number of iterations, N_r. For N_s, the focus is on the accuracy of the *SLP* fit for the early 2010 European cold spell. Several multi-day periods, including the January 1–8 period marked by the occurrence of very cold *TX* anomalies over Europe (Fig. 2a) are used to assess the quality of the *SLP*

495 reconstruction. The dynamical adjustment code is run for a range of N_s values (N_s = 20, 40, 60 …260, 280, 300) keeping the other parameter values to those indicated in the main text. The metric is simply the root-mean square error (RMSE) between the daily original *SLP* and the reconstructed *SLP*. The RMSE is estimated separately for each day and the total RMSE is calculated as the sum in quadrature of the daily RMSE values. Figure A1 shows that the error is systematically large for small N_s values (often greater than 2 hPa for less than 50 analogues), strongly decreases after $N_s \sim 100$ (to less than 1 hPa)

500 and almost saturates to a few tenths of hPa after $N_s \sim 200$ (with RMSEs less than 0.5 hPa beyond $N_s \sim 200$). The shape of the RMSE curve is very similar among the different periods. Note that N_s is a key parameter in term of computational cost as it defines the matrix size involved in the calculation of the Moore-Penrose pseudo-inverse (see Appendix of Deser et al. 2016 for details). Therefore, the choice of $N_s \sim 200$ is a good compromise between accuracy and speed.
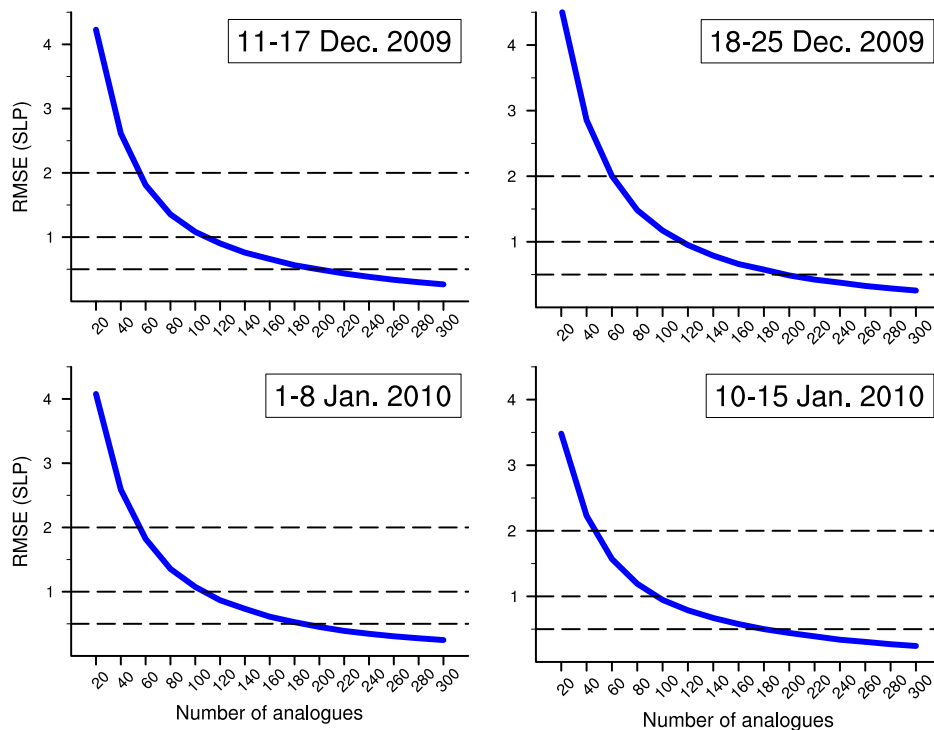
505

Figure A1: Accuracy (assessed by the RMSE, unit: hPa) of the *SLP* reconstruction as a function of the number of analogues used in the dynamical adjustment multilinear regression step. Four multi-day periods (dates in upper-right corner) within the 2010 early winter European cold spell are considered to perform the sensitivity test. The RMSE is first estimated at each grid-point and then averaged over the 30°N–75°N; 25°W–40°E geographical box with latitudinal weighting.

510 The second parameter is the number of iterations, N_r. In this case, the focus is on the reconstructed *TX*. The sensitivity test is performed for several multi-day periods throughout the Russian heat wave. The dynamical adjustment code is run for a range of N_r values (N_r = 10, 20, 30, … 150, 160 and with other parameters at their optimized value) and the metric measures the RMSE between the reconstructed *TX* for the different values in the above N_r range and the reconstructed *TX* field with N_r = 300, taken here as the "reference" value. Note that this only allows to see the "convergence" of the algorithm relative to the

number of iterations for a given value of the N_a and N_s parameters (here $N_a \sim 400$ and $N_s \sim 200$). Figure A2 shows that there is an initial fast RMSE decrease (starting from RMSE values of ~ 1 °C for less than 10 iterations) followed by a slower convergence of the algorithm with the number of iterations. The change in convergence rate occurs when N_r exceeds 50–60 iterations making the choice of $N_r \sim 100$ a reasonable trade-off.
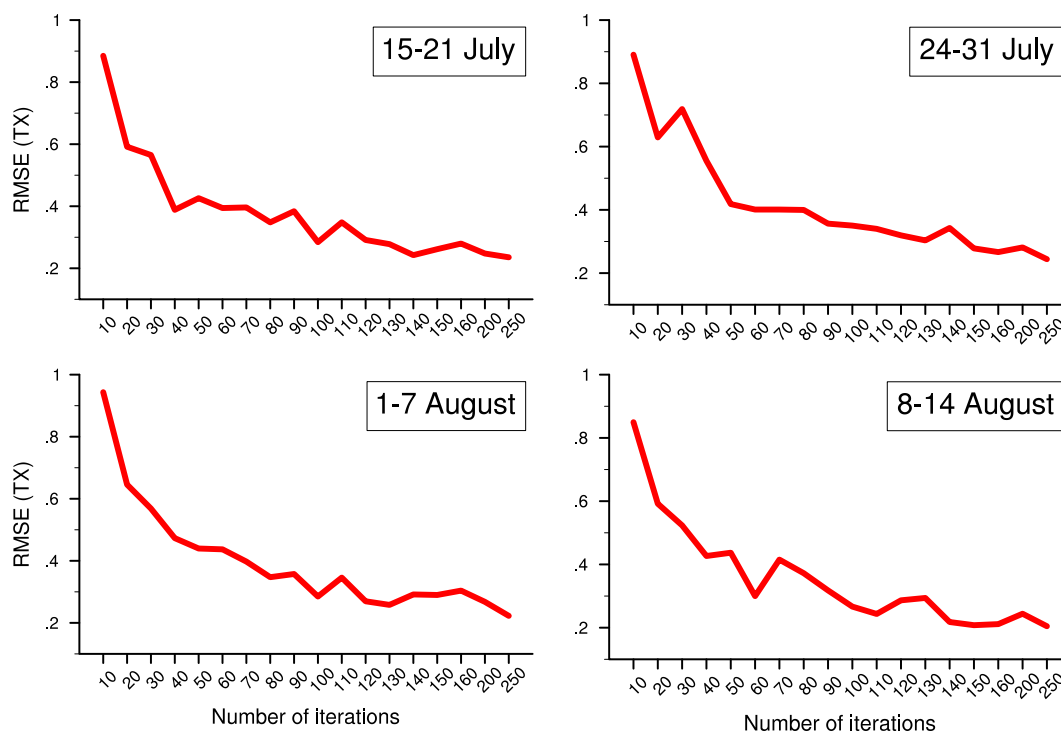
Figure A2: Convergence (assessed by the RMSE, unit: °C) of the *TX* reconstruction as a function of the number of iterations used in the dynamical adjustment algorithm. Convergence is assessed against a reference dynamical adjustment run performed with 300 iterations. Four multi-day periods (dates in upper-right corner) within the 2010 summer Russian heatwave are considered to perform the sensitivity test. The RMSE is first estimated at each grid-point and then averaged over the 35°N–65°N; 25°E–50°E geographical box with latitudinal weighting.

Code and data availability:

The dynamical adjustment code used in this study is available on https://github.com/terrayl/Dynamico. Observed and reanalysis data used for this study can be found on the data provider websites. They can also be provided by the author upon request.

Competing interest:

The author declares no competing interests.

Author contribution:

LT developed the ideas, designed the methodology, developed the computer algorithms, analysed the data, created the figures, and wrote the manuscript.

Acknowledgements: Support for the Twentieth Century Reanalysis Project version 3 dataset is provided by the U.S. Department of Energy, Office of Science Biological and Environmental Research (BER), by the National Oceanic and Atmospheric Administration Climate Program Office, and by the NOAA Physical Sciences Laboratory. The National Center for Atmospheric Research (NCAR) command language (NCL), version 6.5.0, has been used for all the dynamical adjustment computations and visualization of the results.

References

Barriopedro, D., Fischer, E. M., Luterbacher, J., Trigo, R. M., and Garcia-Herrera, R.: The hot summer of 2010: Redrawing the temperature record map of Europe, Science, 332(6026), 220–224, doi:10.1126/science.1201224, 2011

Buchan, J., J. J. Hirschi, A. T. Blaker, and B. Sinha: North Atlantic SST Anomalies and the Cold North European Weather Events of Winter 2009/10 and December 2010. Mon. Wea. Rev., 142, 922–932, doi:10.1175/MWR-D-13-00104.1, 2014

Caesar, J., Alexander, L., and Vose, R.: Large-scale changes in observed daily maximum and minimum temperatures: Creation and analysis of a new gridded data set, J. Geophys. Res., 111, D05101, doi:10.1029/2005JD006280, 2006

Cattiaux, J., Vautard, R., Cassou, C., Yiou, P., Masson-Delmotte, V., and Codron, F.: Winter in 2010 in Europe: A cold extreme in a warming climate. Geophys. Res. Lett., 37, L20704, doi:10.1029/2010GL044613, 2010

Cleveland, R.B., Cleveland, W.S., McRae, J.E., and Terpennings, I.: A Seasonal-Trend Decomposition Procedure Based on Loess. Journal of Official Statistics, Vol. 6, 3–73, 1990

Compo, G. P., and Co-authors: The Twentieth Century Reanalysis Project. Q. J. R. Meteorol. Soc., 137, 1–28, doi:10.1002/qj.776, 2011

Copernicus Climate Change Service (C3S): ERA5: Fifth generation of ECMWF atmospheric reanalyses of the global climate. Copernicus Climate Change Service Climate Data Store (CDS), https://cds.climate.copernicus.eu/cdsapp#!/home, 2017

Cornes, R. C., van der Schrier, G., van den Besselaar, E. J. M., and Jones, P. D.: An Ensemble Version of the E-OBS Temperature and Precipitation Data Sets. J. Geophys. Res. Atmos., 123, 9391–9409, doi:10.1029/2017JD028200, 2018

Dee, D. P., and Co-authors: The ERA-Interim reanalysis: configuration and performance of the data assimilation system. Q. J. R. Meteorol. Soc., 137, 553–597, doi:10.1002/qj.828, 2011

Deser, C., Terray, L., and A. S. Phillips: Forced and internal components of winter air temperature trends over North America during the past 50 years: Mechanisms and implications. J. Climate, 29, 2237–2258, doi:10.1175/JCLI-D-15-0304.1, 2016

Dole, R., Hoerling, M., Perlwitz, J., Eischeid, J., Pegion, P., Zhang, T., Quan, X.-W., Xu, T. and Murray, D.: Was there a basis for anticipating the 2010 Russian heat wave? Geophys. Res. Lett., 38, L06702, doi:10.1029/2010GL046582, 2011

Gong, H., Wang, L., Chen, W., and Wu, R.: Attribution of the East Asian Winter Temperature Trends During 1979–2018:

570   Role of External Forcing and Internal Variability. Geophys. Res. Lett., 46, 10874–10881, doi:10.1029/2019GL084154, 2019

Guan, X., Huang, J., Guo, R., and Pu, L.: The role of dynamically induced variability in the recent warming trend slowdown over the Northern Hemisphere. Sci. Rep., 5, 12669, doi:10.1038/srep12669, 2015

Guo, R., Deser, C., Terray, L., and Lehner, F.: Human influence on winter precipitation trends (1921–2015) over North America and Eurasia revealed by dynamical adjustment. Geophysical Research Letters, 46.

575   https://doi.org/10.1029/2018GL081316, 2019

Guo, Y., and Co-authors: Quantifying excess deaths related to heatwaves under climate change scenarios: A multicountry time series modelling study. *PLOS Med.*, **15**, e1002629, doi:10.1371/journal.pmed.1002629, 2018

Hawkins, E., Frame, D., Harrington, L., Joshi, M., King, A., Rojas, M., and Sutton, R.: Observed emergence of the climate change signal: From the familiar to the unknown. Geophysical Research Letters, 47, e2019GL086259.

580   https://doi.org/10.1029/2019GL086259, 2020

Hersbach, H., Bell, B., Berrisford, P., et al.: The ERA5 global reanalysis. Q. J. R. Meteorol. Soc., 1–51, doi:10.1002/qj.3803, 2020

Horton, D., Johnson, N., Singh, D., Swain, D. L., Rajaratnam, B., and Diffenbaugh, N. S.: Contribution of changes in atmospheric circulation patterns to extreme temperature trends. Nature 522, 465–469, doi:10.1038/nature14550, 2015

585   Hurrell, J. W.: Decadal trends in the north-atlantic oscillation: Regional temperatures and precipitation. Science, 269, 676-679. doi:10.1126/science.269.5224.676, 1995

Jahn, M.: Economics of extreme weather events: Terminology and regional impact models. Weather Clim. Extrem., 10, 29–39, doi:10.1016/j.wace.2015.08.005, 2015

Jézéquel, A., Cattiaux, J., Naveau, P., Radanovics, S., Ribes, A., Vautard, R., Vrac, M. and Yiou, P.: Trends of atmospheric

590   circulation during singular hot days in Europe. Environ. Res. Lett., 13, 054007, https://doi.org/10.1088/1748-9326/aab5da, 2018

Jézéquel, A., Bevacqua, E., d'Andrea, F., Thao, S., Vautard, R., Vrac, M. and Yiou, P.: Conditional and residual trends of singular hot days in Europe Environ. Res. Lett., 15, 064018, https://doi.org/10.1088/1748-9326/ab76dd, 2020

Kalnay, E. et al.: The NCEP/NCAR 40-year reanalysis project. Bull. Am. Meteorol. Soc., 77, 437–471, 1996

595   Lehner, F., Deser, C., Simpson, I., and Terray, L.: Attributing the US Southwest's recent shift into drier conditions. Geophys. Res. Lett., 45. https://doi.org/10.1029/2018GL078312, 2018

Lehner, F., Deser, C., and Terray, L.: Toward a New Estimate of "Time of Emergence" of Anthropogenic Warming: Insights from Dynamical Adjustment and a Large Initial-Condition Model Ensemble. J. Climate, 30, 7739–7756, https://doi.org/10.1175/JCLI-D-16-0792.1, 2017

600   Lloyd, E.A. and Shepherd, T.G.: Environmental catastrophes, climate change, and attribution. Ann. N.Y. Acad. Sci., 1469: 105-124. https://doi.org/10.1111/nyas.14308, 2020

McCarthy, G., and Coauthors: Observed interannual variability of the Atlantic meridional overturning circulation at 26.5°N. Geophys. Res. Lett., 39, L19609, doi:10.1029/2012GL052933, 2012

Miralles, D. G., Teuling, A. J., van Heerwaarden, C. C., and de Arellano, J. V.-G.: Mega-heatwave temperatures due to
605   combined soil desiccation and atmospheric heat accumulation, Nat. Geosci., 7(5), 345–349, doi:10.1038/NGEO2141, 2014

Meredith, E., Semenov, V., Maraun, D. et al.: Crucial role of Black Sea warming in amplifying the 2012 Krymsk precipitation extreme. Nature Geosci 8, 615–619, doi:10.1038/ngeo2483, 2015

Merrifield, A., Lehner, F., Xie, S.-P., and Deser, C.: Removing circulation effects to assess central U.S. land-atmosphere interactions in the CESM Large Ensemble. Geophys. Res. Lett., 44, 9938–9946. https://doi.org/10.1002/2017GL074831,
610   2017

Muller, A., Rohde, R. R., Jacobsen, R., Muller, E., and Wickham, C.: A New Estimate of the Average Earth Surface Land Temperature Spanning 1753 to 2011. Geoinformatics Geostatistics An Overview., 01, doi:10.4172/2327-4581.1000101. http://www.scitechnol.com/2327-4581/2327-4581-1-101.php, 2013

Naveau, P., Hannart, A., and Ribes, A.: Statistical Methods for Extreme Event Attribution in Climate Science. Annual
615   Review of Statistics and Its Application, 7:1, 89-110, 2020

O'Reilly, C. H., Woollings, T., and Zanna, L.: The dynamical influence of the Atlantic multidecadal oscillation on continental climate. J. Climate, 30, 7213–7230, https://doi.org/10.1175/JCLI-D-16-0345.1, 2017

Osborn, T.J.: Winter 2009/2010 temperatures and a record-breaking North Atlantic Oscillation index. Weather, 66: 19-21. doi:10.1002/wea.660, 2011

620   Otto, F. E. L., Massey, N., van Oldenborgh, G. J., Jones, R. G., and Allen, M. R.: Reconciling two approaches to attribution of the 2010 Russian heat wave, Geophys. Res. Lett., 39, L04702, doi:10.1029/2011GL050422, 2012

Otto, F.E.L.: Attribution of Weather and Climate Events. Annu. Rev. Environ. Resour., 42:627–46, doi: 10.1146/annurev-environ-102016-060847, 2017

Robine, J.-M., Cheung, S. L. K., Le Roy, S., Van Oyen, H., Griffiths, C., Michel, J.-P., and Herrmann, F. R.: Death toll
625   exceeded 70,000 in Europe during the summer of 2003. C. R. Biol., 331, 171–178, doi:10.1016/j.crvi.2007.12.001, 2008

Saffioti, C., Fischer, E. M., Scherrer, S. C., and Knutti, R.: Reconciling observed and modelled temperature and precipitation trends over Europe by adjusting for circulation variability. Geophys. Res. Lett., 43:8189–8198, 2016

Schär, C., Kröner, N.: Sequential Factor Separation for the Analysis of Numerical Model Simulations. Journal of the Atmospheric Sciences, 74(5), 1471-1484, doi.org/10.1175/JAS-D-16-0284.1, 2017

630   Schneidereit, A., Schubert, S., Vargin, P., Lunkeit, F., Zhu, X., Peters, D., and Fraedrich, K.: Large scale flow and the long-lasting blocking high over Russia: Summer 2010. Mon. Wea. Rev., 140, 2967-2981, DOI: 10.1175/MWR-D-11-00249.1, 2012

Shepherd, T. G.: A common framework for approaches to extreme event attribution. Curr. Clim. Change

Rep. 2:28–38, 2016

635   Sippel, S., Meinshausen, N., Merrifield, A., Lehner, F., Pendergrass, A. G., Fischer, E. M., and Knutti, R.: Uncovering the forced climate response from a single ensemble member using statistical learning. Journal of Climate, 32, 5677-5699, doi:10.1175/JCLI-D-18-0882.1, 2019

Shaltout, M., Omstedt, A.: Recent sea surface temperature trends and future scenarios for the Mediterranean Sea, Oceanologia, 56, 3, 411-443, doi:10.5697/oc.56-3.411, 2014

640   Slivinski, L. C., Compo, G. P., Whitaker, J. S., et al.: Towards a more reliable historical reanalysis: Improvements for version 3 of the Twentieth Century Reanalysis system. Q. J. R. Meteorol. Soc., 145: 2876– 2908, doi:10.1002/qj.3598, 2019

Smoliak, B. V., Wallace, J. M., Lin, P., Fu, Q.: Dynamical adjustment of the Northern Hemisphere surface air temperature field: Methodology and application to observations. J. Clim. 28:1613–1629, 2015

Sonnewald, M., Hirschi, J. J.-M., Marsh, R., McDonagh, E. L., and King, B. A.: Atlantic meridional ocean heat transport at

645   26° N: impact on subtropical ocean heat content variability, Ocean Sci., 9, 1057–1069, doi:10.5194/os-9-1057-2013, 2013

Squintu, A. A., van der Schrier, G., Brugnara, Y., and Klein Tank, A.: Homogenization of daily temperature series in the European Climate Assessment & Dataset. Int. J. Climatol., 39, 1243–1261, doi:10.1002/joc.5874, 2019

Stillman, J. H.: Heat Waves, the New Normal: Summertime Temperature Extremes Will Impact Animals, Ecosystems, and Human Communities. Physiology, 34, 86–100, doi:10.1152/physiol.00040.2018, 2019

650   Stott, P. A., Stone, D. A., and Allen, M. R.: Human contribution to the European heatwave of 2003. Nature, 432, 610–13, 2004

Stott, P., Christidis, N., Otto, F., Sun, Y., Vanderlinden J., et al.: Attribution of extreme weather and climate-related events. WIREs Clim. Change 7:23–41, 2016

Van Garderen, L., Feser, F., and Shepherd, T. G.: A methodology for attributing the role of climate change in extreme

655   events: a global spectrally nudged storyline. Nat. Hazards Earth Syst. Sci., 21, 171–186, 2021, doi.org/10.5194/nhess-21-171-2021, 2021

Vautard, R., Yiou, P., Otto, F., Stott, P., Christidis, N., van Oldenborgh, G. J., and Schaller, N.: Attribution of human-induced dynamical and thermodynamical contributions in extreme weather events. Environ. Res. Lett. 11, 114009, 2016

Wallace, J. M., Fu Q., Smoliak, B.V., Lin, P., and Johanson, C. M.: Simulated versus observed patterns of warming over the

660   extratropical Northern Hemisphere continents during the cold season. Proc. Natl. Acad. Sci., 109, 14337–14342, 2012

Wang, C., Liu, H., and Lee, S-K.: The record-breaking cold temperatures during the winter of 2009/2010 in the Northern Hemisphere. Atmos. Sci. Let. 11: 161–168, doi: 10.1002/asl.278, 2010

Wehrli, K., Guillod, B. P., Hauser, M., Leclair, M., & Seneviratne, S. I.: Identifying key driving processes of major recent heat waves. Journal of Geophysical Research: Atmospheres, 124, 11,746–11,765, doi: 10.1029/2019JD030635,

665   2019

Woollings, T., Papritz, L., Mbengue, C., and Spengler, T.: Diabatic heating and jet stream shifts: A case study of the 2010 negative North Atlantic Oscillation winter. Geophys. Res. Lett., 43, 9994–10,002, doi:10.1002/2016GL070146, 2016